COMPARISON OF NEUTRON, PROTON AND GAMMA RAY EFFECTS IN SEMICONDUCTOR DEVICES*

J.P. Raymond
Mission Research Corporation
San Diego, CA

E.L. Petersen
Naval Research Laboratory
Washington, DC

ABSTRACT

Interest in proton radiation effects has intensified in recent years. A prime focus is the relationship between proton displacement and ionization effects and the separate consideration of neutron-induced displacement and gamma-ionization effects in TREE characterization. Recent definitive work on proton and neutron displacement damage in silicon in terms of nonionizing energy loss has laid the groundwork for comparison of proton effects with the TREE data base. We initiate this comparison with a summary of device radiation susceptibilities in neutron and gamma environments. Proton interactions in silicon devices are then presented in terms of dose deposition and nonionizing energy loss. This leads to a neutron-proton damage equivalence factor and enables the development of simple correspondence. The device susceptibility charts are then combined so both displacement damage and ionization-damage can be schematically examined relative to proton dose. These susceptibility charts demonstrate the dominance of ionization effects for damage in a proton environment for modern silicon microcircuit technologies. This approach is presented as a convenient means of interpreting effects for both proton exposures and TREE simulators. It is concluded that TREE characterization can be used as a good first-order estimate of proton damage effects.

1. INTRODUCTION

In the assessment of proton-induced damage to silicon microcircuits, it would be very useful to draw from the knowledge gained from the study of transient radiation effects on electronics (TREE) over the last 25 years. Extensive facilities have been built to enable the assessment of performance degradation effects in semiconductor devices resulting from neutron-induced atomic displacements and gamma-ray-induced ionization. The existing TREE data base would be applicable to proton effects assessment, given correlation of displacement damage and ionization effects. In addition, given correlation, the number of facilities available for proton damage assessment can be expanded to include the TREE simulation facilities as well as available cyclotrons.

Correlation of proton damage effects to both neutron displacement damage and ionizing radiation exposure has been established by a number of basic material and device studies [1-4]. In this paper the correlation will be interpreted in terms of device TREE susceptibility. This interpretation clearly indicates that long-term ionization effects are the primary damage mechanism for proton exposure of virtually all types of modern silicon microcircuits.

2. DEVICE SUSCEPTILBIITY ASSESSMENT

Characterization of displacement and long-term ionization damage effects on semiconductor piece-parts is routine in the support of the development of systems which must be hardened to nuclear weapon and space radiation environments. Typically, it is assumed that the displacement damage and ionization effects are independent, so that damage characterizations can be done separately. The facilities used to characterize TREE are a pulsed nuclear reactor for the neutron source, and a Cobalt-60 source or electron accelerator (e.g., Dynamitrons, linear accelerators, Van de Graaff generators) for the ionization source.

2.1 Neutron Displacement Damage

The exposure environment of a pulsed nuclear reactor includes high-energy neutrons and concomitant gamma rays. A comprehensive characterization of semiconductor device effects includes the time dependent nature of neutron displacement damage and ionization as potential failure mechanisms. The device(s) under test would be actively biased during exposure, the test conditions would be carefully selected, and the response(s) would be monitored during and after exposure. Fortunately, however, if only characterization of stable neutron displacement damage effects is of interest there is virtually no dependence of the result on the test conditions during exposure, and devices are routinely exposed with no electrical connection (usually with all external leads shorted in conductive foam).

In terms of the radiation effects data base, neutron damage susceptability is most frequently reported in terms of neutron fluence at the failure level observed after a series of reactor exposures. Results of these characterizations can be summarized as a range of device susceptibility for major microcircuit technologies as shown in Figure 1. Neutron failure levels for the MOS technologies are estimated based only on displacement damage effects. The first order effect in n-MOS technologies is the degradation of minority carrier lifetime, which increases critical leakage currents in high-performance arrays. The estimate of critical displacement damage effects in bulk CMOS is based on reported limitations in the use of neutron exposure to reduce lifetime and increase latchup hardness [5,6]. The estimate of critical displacement damage effects on CMOS/SOS microcircuits is based on relatively early evaluations. In recent years it has been assumed that the hardness is dominated by ionization-induced damage [7].

Neutron failure levels for bipolar microcircuit technology reflect the sensitivity of circuit performance to the dominant degradation in transistor common-emitter gain, as well as the evolution to

*Work was partially sponsored by the LTH-4.2 Program through Naval Research Laboratory Contract N00014-85-C-2642.

0018-9499/87/1200-1622$01.00 © 1987 IEEE

transistors with higher gain-bandwidth products and thus lower neutron damage susceptibility [8]. The failure levels for the TTL microcircuits reflect relatively old gold-doped devices in which minority carrier lifetime degradation is not critical. The evolution to non-gold-doped Low-Power TTL results in greater sensitivity to minority carrier lifetime degradation and an increasing dependence on relatively high transistor gains with advances in processing control. The high neutron failure levels of both Junction-Isolated ECL and all oxide-separated bipolar digital circuit technologies reflects the application of very high gain-bandwidth transistor elements. The neutron susceptibility of ECL is slightly reduced because of the trend to depend on relatively high transistor gains. The neutron susceptibility of analog bipolar is shown as a very broad range because the failure level reflects both a substantial variation in process technology and depends critically on the demands of the performance requirements. The failure level for a very precise, high performance analog device will be much less than that of the analog device in an applicaiton that allows substantial degradation of the performance parameters.

The estimated ranges of microcircuit neutron damage susceptibility are shown in the traditional bar chart form in Figure 1 (Refs. 8, 9). The specific ranges of the estimated susceptability may be, and typically are, the source of significant debate. However, our purpose is to focus attention on the ranges of susceptibility rather than legislate specific boundaries.

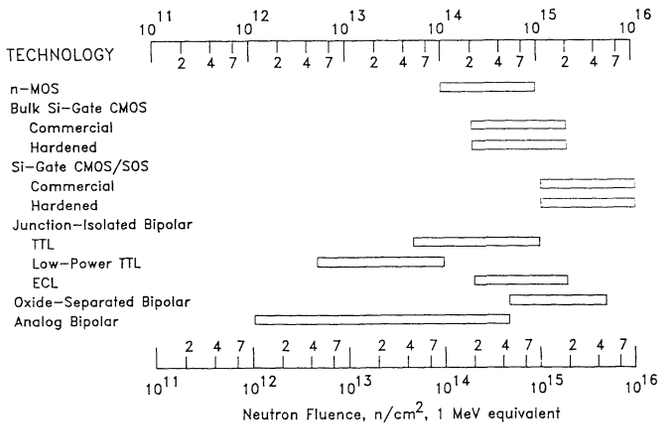

Figure 1. Estimating ranges of microcircuit neutron damage susceptibility.

2.2 Long-term Ionization Damage

The characterization of long-term ionization damage is typically performed by exposure to gamma rays from a Cobalt-60 source or high energy electrons from an accelerator. The complexities of determining the system-dependent failure level of a given device are legion. They include strong dependence on the electrical bias conditions during exposure, the radiation intensity during exposure, the gamma ray/electron energy spectrum at the device, electrical bias after exposure, and measurement time after exposure. Currently, the techniques and facilities for exposing devices and measuring a failure level in the laboratory environments are well known. Unfortunately, it is often difficult to apply the laboratory simulation failure data to determine the device operational failure level. In this paper we will consider the TREE data base as it exists in terms of reported failure levels for laboratory exposures.

2.2.1 Cobalt-60 Exposure

Exposure of a semiconductor device to the gamma rays from a Cobalt-60 source is a popular and relatively inexpensive method of determining ionizing radiation damage susceptibility. Typically, the devices under test are electrically biased and are either monitored during exposure (i.e., in situ) or characterized by removal from the cell at defined intervals. The reported failure level for the device is generally reported in rads(Si), which is interpreted as essentially equal to the energy deposition by ionization in the silicon-dioxide gate insulator and surface passivation regions. Gamma ray exposure does produce displacment damage in the bulk semiconductor through the resultant Compton electrons. For all practical purposes, in modern semiconductor devices the gamma ray-induced displacment damage effects are negligible compared to the long-term-ionization effects.

2.2.2 High-Energy Electron Exposure

High-energy electron exposure is a very popular approach, also used for simulation of the electron exposure of the natural space environment. The facilities used for simulation are principally Dynamitrons. A major source of radiation effects data is the JPL Voyager/Galileo Data Bank that includes results of both electron and Cobalt-60 gamma exposure [10,11]. Failure levels resulting from the electron exposure are reported either in terms of rads(Si) or electrons/cm^2. In the JPL data a conversion factor of 4 x 10^7 e/cm^2 per rad(Si) is used for the 2 MeV electron exposure of the Dynamitron facility. It should be noted that high-energy photon electron exposure can cause displacement damage that may be important for very sensitive devices such as some bipolar analog microcircuits.

2.2.3 Reported Ranges of Device Susceptibility

The failure levels observed in Cobalt-60 and high-energy electron environments can be presented as ranges of susceptibility by technology as shown in Figure 2 [8, 10-14]. In addition to all the caveats noted in the discussion of neutron failure level summaries, the long-term-ionization ranges must include the significant variation of failure with bias/time conditions and the variation between high-performance commercial technologies and radiation-hardened technologies. The lower limit on long-term ionization hardness is for high-performance n-MOS microcircuits and is on the the order of 1 krad(Si). The hardness of commercial CMOS is significantly greater than that of n-MOS because of the increased tolerance of CMOS circuits to radiation-induced threshold voltage shifts. The distinction between high-performance commercial and hardened CMOS is in variations of fabrication processes, process control, and circuit design which, in total, can increase the hardness by two orders of magnitude or greater. The hardness of commercial CMOS/SOS is somewhat less than that of bulk CMOS because of charge trapping effects at the additional oxide-semiconductor interfaces. Again, hardened CMOS/SOS is distinguished by process and circuit design techniques for hardness and hardness assurance even perhaps at some performance penalty.

For many years it had been reasonable to assume that the long-term-ionization hardness of digital bipolar technologies was very high and therefore of little concern. That position is reasonable for relatively highly-doped junction-isolated digital

bipolar circuits where the failure mechanism is transistor gain degradation. The advent of oxide-separation techniques, which have practically displaced the older junction-isolated technology, introduced circuit failure due to surface inversion under the oxide-separation isolation regions. As a result, the "total-dose" hardness of the digital and analog oxide-separated bipolar technologies is substantially less than that of the earlier junction-isolated devices. As with other technologies, the lower limit of the susceptibility range represents commercial technology optimized for yield and performance, and the upper range includes circuits that have been fabricated with considerations of radiation susceptibiltiy.

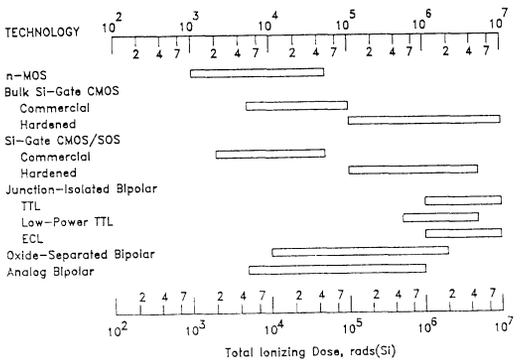

Figure 2. Estimated ranges of microcircuit long-term ionizing radiation damage.

As with neutron damage, the range of susceptiblity for analog bipolar technologies is very wide because of the range of fabrication processes and performance requirements. Significant long-term ionizing radiation susceptibility can be observed in any technology for very demanding performance requirements. The JPL/Galileo Data Base includes data on a wide variety of analog circuit types, as well as the observed variations in the hardness of a specific product with procurement history and with efforts in hardening. As with neutron damage effects, the ranges of ionizing radiation damage susceptibility can be debated at some length. The purpose of this work, however, is to suggest these as representative of the existing data base in order to illustrate the related effects of high-energy proton exposure.

2.3 Schematic Representation of Microcircuit Susceptibility

In order to relate proton effects to the TREE data base on neutron and ionization damage it will be convenient to combine the estimated ranges of susceptibility shown in Figures 1 and 2 into a two-dimensional schematic form as shown in Figure 3. In Figure 3, the ranges of displacement damage susceptibility are along the ordinate, and the ranges of ioniziation damage susceptibility are along the abscissa. The one-dimensional susceptibility ranges of the bar charts now become two-dimensional regions of susceptibility. It must be emphasized that this plot does not imply that the neutron fluence is the dependent variable and that ionization is the independent variable, but rather is a schematic convenience. In Sections 3 and 4 we will develop the concept as a convenience in examining displacement damage and ionization in both proton and TREE simulation environments.

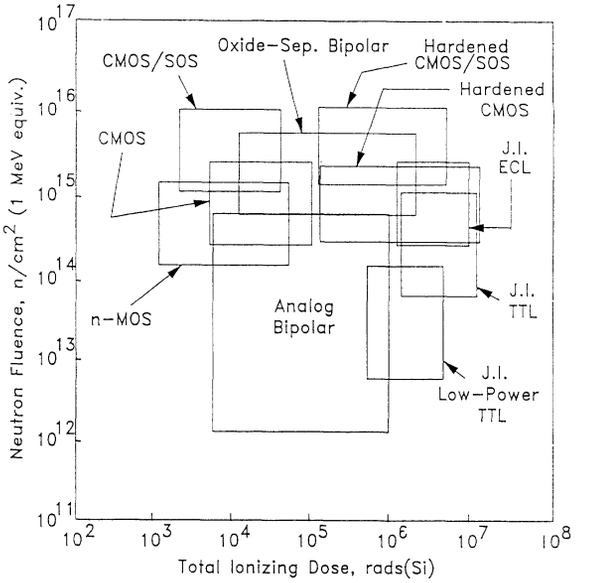

Figure 3. Schematic representation of microcircuit susceptibility.

3. HIGH ENERGY PROTON EFFECTS

High energy proton exposure differs from the traditional TREE exposures in that the energy deposition goes into both displacement and ionization processes. Previous studies have carefully considered the potential equivalence of the resulting effects, both analytically and experimentally [1-4].

3.1 Proton Ionization

Proton energy loss due to ionization dominates most proton effects in materials. Incident protons lose energy through inelastic collisions with bound electrons in the atoms and molecules of the stopping material and results in their ionization and excitation. Above 1 MeV the proton energy loss by ionization and excitation can be calculated using the Bethe equation [15]. The specific energy loss (dE/dx) is ordinarily expressed in units of MeV/g/cm^2. Energy loss can be directly converted into ionizing dose delivered. The dose is the amount of energy deposited per unit mass, and is the product of dE/dx time the fluence, Φ, (p/cm^2). The ionization dose can be calculated from,

$$D = 1.6 \times 10^{-8} \frac{\text{rads - g}}{\text{MeV}} \cdot \frac{dE}{dx} \cdot \Phi$$

The ionization dose per unit fluence is plotted as a function of energy in Figure 4 (right scale), based on the values of dE/dx calculated by Janni [15].

3.2 Proton Nonionizing Energy Loss

The proton nonionizing energy loss includes four effects [1]. These are the elastic coulomb scattering of protons by the field of the nuclei, nuclear elastic scattering, inelastic nuclear scattering and reactions, and Lindhard energy partition. The nonionizing energy loss again has units of Mev/g/cm^2. Burke [1] calculated the energy dependence of proton nonionizing energy loss, usin gthe most recent data. He then calculated the ratio of proton nonionizing energy loss to 1 MeV neutron nonionizing enrgy loss (2.04×10^{-3} MeV/g/cm^2 obtained from the neutron damage factor, K_n = 95 MeV-mb) [2]. There is

excellent agreement of the calculated ratio of non-ionizing energy with the measured ratio of neutron to proton damage factor (K_p/K_n) [3,16]. The ratios appear to be identical. Figure 4 shows the energy dependence of the displacement damage factor (K_p/K_n) plotted against the left ordinate. It should be noted from this graph that both ionizing and non-ionizing energy losses have similiar energy dependence. They both decrease with increasing proton energy, and the ratio remains nearly constant.

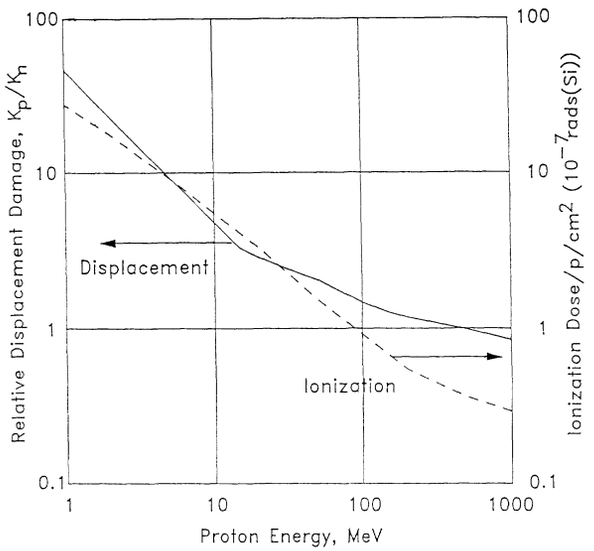

Figure 4. Proton energy deposition.

3.3 Neutron/Proton Damage Equivalence Factors

The proton and neutron damage factors relate the displacement damage to the particle fluence, Φ_p and Φ_n. It would be convenient to know the neutron fluence that is equivalent (as far as displacement damage is concerned) to a given proton dose. This can be obtained from the information in Figure 4. One curve shows the ratio of proton to neutron damage as a function of proton energy. The other curve shows the dependence of ionizing dose on proton energy. The ratio of the two curves then relates neutron to proton displacement damage as a function of dose (D), by a factor (R_p) defined as,

$$R_p = \frac{K_p/K_n}{D/\Phi_p}$$

For equivalent damage,

$$K_n\Phi_n = K_p\Phi_p$$

$$\Phi_n = \frac{K_p}{K_n}\,\Phi_p$$

$$= \frac{K_p/K_n}{D/\Phi_p} \cdot D$$

$$\Phi_n = R_p \cdot D$$

Figure 5 shows the neutron-proton damage equivalence factor (R_p) as a function of proton energy. The neutron fluence corresponding to a given dose delivered at a given proton energy is determined by the factor R_p at that proton energy. Clearly, R_p varies little over a wide range of proton energies. If one chooses a reference R_p at 90 ($R_p(90) = 1.54 \times 10^7$), the geometric means of the extremes, R_p is always within a factor of two at any other energy. 90 MeV is also a convenient reference as 10^7 p/cm^2 delivers one rad(Si).

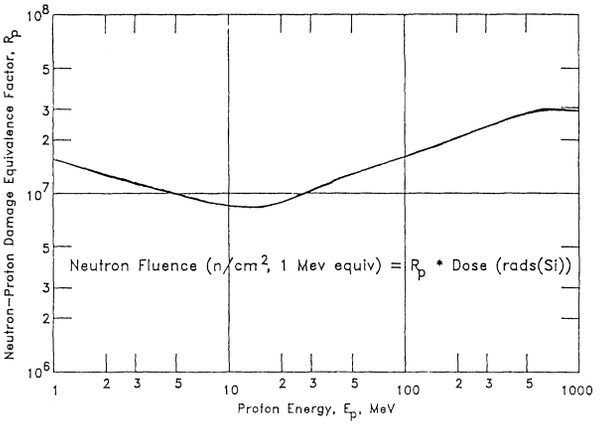

Figure 5. Relative proton displacement and ionization.

3.4 Proton Effects Schematic Development

It is interesting to plot the neutron fluence as a function of proton ionizing dose. This is done in Figure 6 for 90 MeV protons and for the extremes of 14 MeV ($R_p = 8.2 \times 10^6$) and 800 MeV ($R_p = 2.9 \times 10^7$). The extremes determine a relatively narrow band and the neutron-proton equivalence is within this band for all proton energies. Figure 6 corresponds in form to Figure 3 with neutron fluence on the ordinate and dose on the abscissa. This suggests that failure data can be directly plotted on Figure 6 for susceptibility in a proton environment. One question that needs to be considered about total ionizing dose damage is the problem of the equivalence of damage by gamma rays (Co-60), protons, and other ionizing particles which arises because of the different ionization densities. This has been studied by several authors [17-23]. The best single set of experiments was that of Tallon and coworkers [22]. The basic conclusion of these groups was that under some conditions protons are less damaging (i.e., cause less transistor threshold shift) than gamma rays for proton energies less than 25 MeV. The differences disappear for devices not under bias or for protons incident at 45 degrees. The measurements are greatly complicated by the normal post irradiation effects of dependence on dose rate and annealing time. There currently are no gamma-proton comparisions made with separation of interface states and hole trapping processes. There are still a number of questions about the details of dose equivalence.These include variations in post-irradiation-effects due to exposure times. The exposure times of interest range from the high-intensity flash x-ray pulse to the low-intensities of Cobalt-60 exposure with pulsed neutron/proton exposures between the limits.

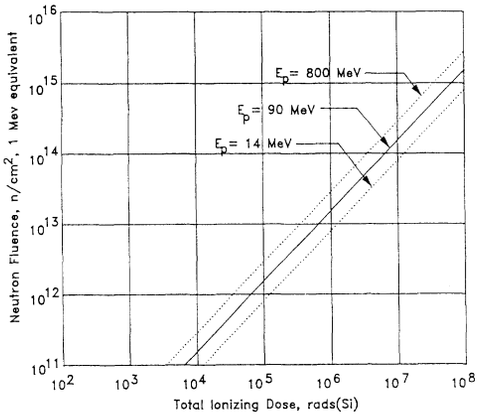

Figure 6. Representation of proton effects.

At the present it appears that a valid conservative approach is to assume that gamma total ionizing dose damage and proton total ionizing dose damage are equivalent. The exceptions occur only at low proton energies for some angles of incidence and for some operating conditions. With this caveat, the dose axis on Figure 6 can be assumed to apply for either proton or gamma dose. In Figure 3, the ranges of microcircuit susceptibility were shown as regions for each technology in terms of independent characterizations of neutron displacement damage and ionizing radiation damage. In Figure 6, proton energy deposition is presented in terms of ionization and the corresponding displacement damage in terms of 1 MeV neutron fluence. Since Figures 3 and 6 both have the same scales, they can be overlayed as shown in Figure 7. The result is a schematic in which we can compare proton effects to the TREE neutron/gamma data base.

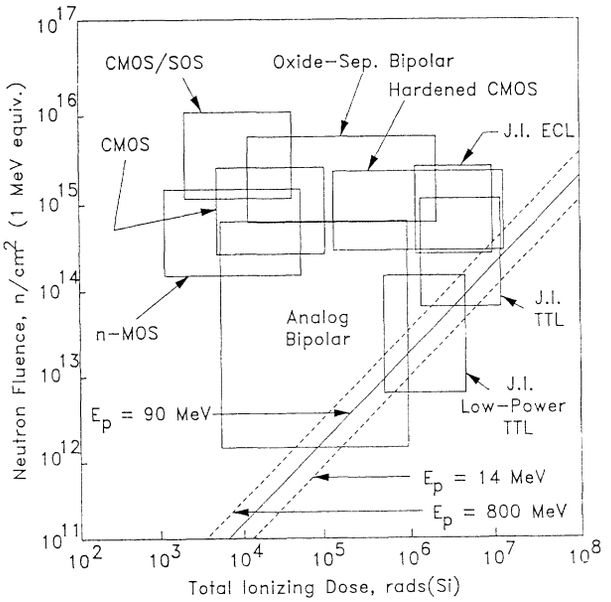

Figure 7. Schematic representation with proton effects.

4. INTERPRETATION OF DEVICE SUSCEPTIBILITY

4.1 Proton Suceptibility

The failure level of any particular device can be shown as a point on Figure 7. For a proton exposure, the increasing fluence corresponds to a cursor moving along the equivalance line with corresponding vertical and horizontal lines defining accumulated dose and equivalent neutron fluence. When the cursor reaches a point such that either line exceeds the associated radiation tolerance, the device fails. If the device fails at high gamma dose and low neutron fluence, the failure point will be in the region of susceptibility which is to the lower right of the proton equivalence band, and failure in a proton exposure would be governed by displacement damage. If the device fails at low dose and high neutron fluence, the point falling to the upper left of the equivalence band, its failure in a proton exposure would be due to total ionizing dose effects.

For example, consider the interpretation for commercial CMOS technology as shown in Figure 7. In terms of total ionizing radiation exposure, the failure range for commercial CMOS is approximately from 5,000 to 100,000 rads(Si), or at the lower range of proton ionization as shown in Figure 7. On the other hand, the displacement damage range for commercial CMOS is on the order of 2×10^{14} to 2×10^{15} n/cm^2, which corresponds to a neutron exposure at the upper end of the proton exposure range as shown in Figure 7. In this case, it is clear that the susceptibility of the technology in a high energy proton exposure will be dominated by ionization damage. The role of ionization damage in commercial CMOS hardness is certainly no surprise, but the same observation for the other microcircuit technologies shown in Figure 7 is interesting. In general, if the region of microcircuit susceptibility as shown in Figure 7 is above the proton equivalent line, its hardness is dominated by ionization damage. Conversely, if the region is below the proton equivalent line, its hardness is dominated by displacement damage.

The increased importance of ionization damage as the principal failure mechanism in proton exposures compared to TREE has been noted previously (Ref. 24), particularly for the MOS technologies. In the schematic form of Figure 7, however, in addition to the identification of the failure mechanism, one can estimate the degree of dominance and thus the sensitivity to particular part selection within the technology family as well as the sensitivity to proton energy. For example, for the junction-isolated bipolar technologies, the regions of susceptibility are near the proton equivalence line, and while ionization damage dominates in many cases, the failure mechanism should be assessed for the specific part type of interest and for the specific proton energies of interest. It is interesting to note, however, the clear dominance of ionization damage in oxide isolated bipolar technology. With the relatively high neutron hardness of the technology, it is clear that ionization damage will be the primary failure mechanism for any specific device in the technology family and for any proton energy.

4.2 Combined Neutron/Gamma Susceptibility

It should be noted, however, that the application of the TREE data base to proton effects still contains some implicit assumptions and unanswered questions. In the determination of the neutron damage susceptibility it is generally assumed that the TREE results are dominated by displacement

damage. In Figure 8, the ionization associated with neutron exposure has been added to the schematic. The line for the "Typical Reactor Exposure" represents the concomitant gamma ionization associated with the neutron exposure for a SPR-III reactor facility [25]. Since the estimates of microcircuit susceptibility regions are based on independent characterizations of displacement and ionization damage the specific test conditions of the reactor exposure must be considered. The comparison to either the neutron/reactor or proton equivalence lines is valid when the devices are exposed under active bias test conditions representing a reasonable worst case for ionization effects. With the devices unbiased it is typically assumed that the effects are dominated by displacement damage. The assumption can be checked by measurement of the relative effects in the neutron or proton environment against comparable measurements in a gamma or high-energy electron environment. For example, in comparing the reactor exposure line to the microcircuit susceptibility regions, displacement damage is the dominant failure mechanism for some of the bipolar technologies, ionization damage under active bias is the dominant failure mechanism for the MOS and some of the bipolar technologies. It is also interesting to note that evolution in the development of CMOS hardened to ionization damage can result in an increase in displacement damage effects for high-energy proton exposures.

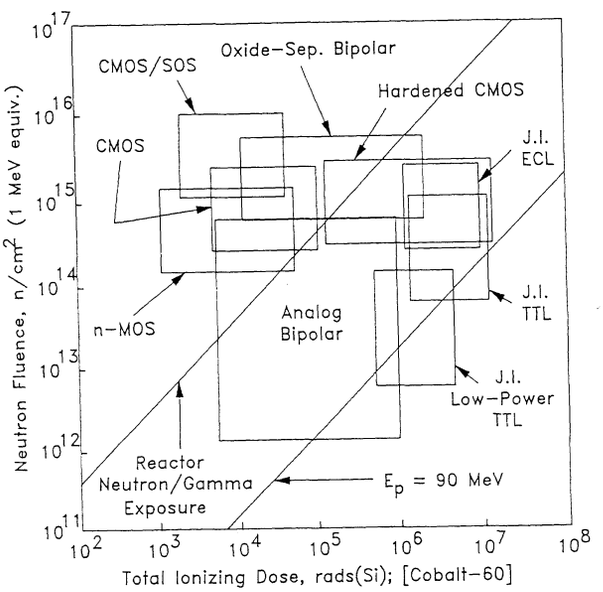

Figure 8. Scehmatic with proton, reactor effects.

5. SUMMARY

A schematic representation combining TREE damage susceptibility and high-energy proton effects has been developed. We have used estimates from the TREE data base and recently developed equivalences of proton and neutron displacement damage utilizing the concept of nonionizing energy loss. The resulting neutron-proton damage equivalence function is used to directly relate proton-induced displacement damage to 1 MeV equivalent neutron displacement damage. The schematic representation presenting both ionization and displacement damage is a useful guide when studying proton effects. For example, it is clear that, to a first order, the TREE data base can be used directly in evaluating proton induced damage susceptibility. TREE data, however, will generally not be available for the evaluation of new or unique silicon devices. In this case, TREE laboratory simulation facilities can be used to obtain new test data that will give a first order estimate of susceptibility in proton environments. For most current silicon technologies, only gamma or electron exposures are needed, as the total ionization damage effects dominate the displacement damage effects. In many cases, adequate proton damage estimates can be made without undertaking a specific proton effects characterization.

There are a number of situations where direct proton testing will still be needed. There are possibilities of heating or synergistic effects at high proton fluxes. The high dose rates also present new problems with the various classes of effects grouped as post-irradiation effects. The results presented here are for the traditional rates of dose application and do not necessarily apply under extremely low or extremely high dose rates. There are a large number of uncertainties about relative gammaproton effects at low proton energies. These can be important in the space environment. The results and approaches developed in this paper allow a quick appraisal of the value of the traditional TREE testing and the needs for new proton testing.

ACKNOWLEDGEMENT

The authors wish to express their gratitude for the encouragement and support of Ed Burke and Geoff Summers.

REFERENCES

1. E.A. Burke, "Energy Dependence of Proton-Induced Displacement Damage in Silicon, IEEE Trans. on Nuclear Science, vol. NS-33, no. 6, pp. 1276-1281; December, 1986.

2. G.P. Summers, E.A. Wolicki, M.A. Xapsos, P. Marshall, C.J. Dale, M.A. Gehlhausen and R.D. Blice, "Energy Dependence of Proton Displacement Damage Factors for Bipolar Transistors," IEEE Trans. on Nuclear Science, vol. NS-33, no. 6, pp. 1282-1286; December, 1986.

3. G.P. Summers, E.A. Burke, C.J. Dale, E.A. Wolicki, P. Marshall and M. Gehlhausen, "Correlation of Particle-Induced Displacement Damage in Silicon," presented at the 1987 IEEE Nuclear and Space Radiation Effects Conference, Snowmass, Colorado; July, 1987.

4. V.A.J. van Lint, G. Gigas and J. Barengoltz, "Correlation of Displacement Effects Produced by Electrons, Protons, and Neutrons in Silicon," IEEE Trans. on Nuclear Science, vol. NS-22, no. 6, pp. 2663-2668; December, 1975.

5 J.R. Adams and R.J. Sokel, "Neutron Irradiation for Prevention of Latch-up in MOS Integrated Circuits," IEEE Trans. on Nuclear Science, vol. NS-26, no. 6, pp. 5069-5073; December, 1979.

6. J.E. Schroeder, A. Ochoa, Jr., and P.V. Dressendorfer, "Latch-up Elimination in Bulk CMOS LSI Circuits," IEEE Trans. on Nuclear Science, vol. NS-27, no. 6, pp. 1735-1738; December, 1980.

7. G.J. Brucker, "Transient and Steady-State Response of CMOS/SOS," IEEE Trans. on Nuclear for Science, vol. NS-27, no. 6, pp. 1674-1679; December, 1980.

8. D.M. Long, "Hardness of MOS and Bipolar Integrated Circuits," IEEE Trans. on Nuclear Science, vol. NS-27, no. 6, pp. 1674-1679; December, 1980.

9. J.P. Raymond, "MSI/LSI Radiation Response, Characterization and Testing," IEEE Trans. on Nuclear Science, vol. NS-21, no. 6, pp. 308-314; December, 1974.

10. W.E. Price, K.E. Martin, D.K. Nichols, M.K, Gauthier, S.F. Brown, "Total-Dose Radiation Effects Data for Semiconductor Devices," JPL Publication 81-66; December 1, 1981.

11. K.E. Martin, M.K. Gauthier, J.R. Coss, A.R.V. Dantas, W.E. Price, "Total-Dose Radiation Effects Data for Semiconductor Devices, 1985 Supplement," JPL Publication 85-43, October, 15, 1985.

12. D.K. Myers, "Radiation Effects on Commerical Semiconductor 4 Kilobit Memories," IEEE Trans. on Nuclear Science, vol. NS-23, no. 6, pp. 1732-1737; December, 1976.

13. D.G. Cleveland, "Dose Rate Effects in MOS Mircocircuits," IEEE Trans. on Nuclear Science, vol. NS-31, no. 6, pp. 1348-1353; December, 1984.

14. R.L. Pease, R.M. Turfler, D. Platteter, D. Emily and R. Blice, "Total Dose Effects in Recessed Oxide Digital Bipolar Microcircuits," IEEE Trans. on Nuclear Science, vol. NS-30, no. 6, pp. 4216-4223; December, 1983.

15. J.F. Janni, "Proton Range-Energy Tables," Atomic Data and Nuclear Data Tables, vol. 27, p. 341; 1982.

16. R.L. Pease, E.W. Enlow and G.L. Dinger, "Comparison of Proton and Neutron Carrier Removal Rates," presented at the 1987 IEEE Nuclear and Space Radiation Effects Conference, Snowmass, Colorado; July, 1987

17. T.R. Oldham and J.M. McGarrity, "Ionization of Silicon-Dioxide by Heavy Charged Particles," IEEE Trans. on Nuclear Science, vol. NS-28, no. 6, ppp. 3968-3974; December, 1981.

18. G.J. Brucker, E.G. Stassinopoulos, O. van Gunten, L.S. August and T.M. Jordan, "The Damage Equivalence of Electrons, Protons, and Gamma Rays in MOS Devices," IEEE Trans. on Nuclear Science, vol. NS-29, no. 6, pp. 1966-1969; December, 1982.

19. G.J. Brucker, O. Van Gunten, E.G. Stassinopoulos, P. Shapiro, L.S. August, T.M. Jordan, "Recovery of Damage in Rad-Hard MOS Devices During and After Irradiation by Electrons, Protons, Alphas, and Gamma Rays," IEEE Trans. on Nuclear Science, vol. NS-30, no. 6, pp. 4162-4168; December, 1983.

20. E.G. Stassinopoulos, G.J. Brucker, O. van Gunten, "Total-Dose and Dose-Rate Dependence of Proton Damage in MOS Devices During and After Irradiation," IEEE Trans. on Nuclear Science, vol. NS-31, no. 6, pp. 1444-1447; December, 1984.

21. T.R. Oldham, "Analysis of Damage in MOS Devices for Several Radiation Environments," IEEE Trans. on Nuclear Science, vol. NS-31, no. 6, pp. 1236-1241; December, 1984.

22. R.W. Tallon, M.R. Ackermann, W.T. Kemp, M.H. Owen and D.P. Saunders, "A Comparison of Ionizing Radiation Damage in MOSFETs from Cobalt-60 Gamma Rays, 0.5 to 22 MeV Protons and 1 to 7 MeV Electrons," IEEE Trans. on Nuclear Science, vol. NS-32, no. 6, pp. 4393-4398; December, 1985.

23. W.J. Stapor, L.S. August and D.H. Wilson, "Proton and Heavy-Ion Radiation Damage Studies in MOS Transistors," IEEE Trans. on Nuclear Science, vol. NS-32, no. 6, pp. 4399-4404; December, 1985.

24 D.R. Locker, et al., "The Present State of Hardness of Electronic Devices and Sensor Types to High Energy Protons," Air Force Weapons Laboratory Technical Report AFWL-TR-81-81; January, 1982.

25. L.M. Choate and T.R. Schmidt, "New Neutron Simulation Capabilities Provided by the Sandia Pulse Reactor-III (SPR-III) and the Upgraded Annular Core Pulse Reactor (APCR)," IEEE Trans. on Nuclear Science, vol. NS-25, no. 6, pp. 1625-1628; December, 1978.